Available online at www.sciencedirect.com
SCIENCE DIRECT®
International Journal of Thermal Sciences 43 (2004) 213–220
International Journal of Thermal Sciences
www.elsevier.com/locate/ijts

Forced convection past a heated cylinder in a porous medium using a thermal nonequilibrium model: Finite Péclet number effects

W. Sam Wong [a,1], D. Andrew S. Rees [a,*], Ioan Pop [b]

[a] *Department of Mechanical Engineering, University of Bath, Claverton Down, Bath, BA2 7AY, UK*
[b] *Faculty of Mathematics, University of Cluj, 3400 Cluj, CP253, Romania*

Received 7 April 2003; accepted 2 July 2003

Abstract

We study the forced convective heat transfer from a uniform temperature cylinder placed perpendicular to an otherwise uniform fluid stream in a porous medium at finite values of the Péclet number. Attention is focused on how the absence of local thermal equilibrium between the solid and fluid phases affects the temperature fields of the two phases and the rates of heat transfer from the cylinder. Detailed numerical results are given for a wide range of parameter values. On the upstream side of the cylinder the temperature field extends further from the cylinder in the solid phase than it does for the fluid phase, but the opposite is true on the downstream side.

Keywords: Forced convection; Porous media; Local thermal nonequilibrium; Cylinder; Finite Péclet number

1. Introduction

Local thermal equilibrium in porous media is a state whereby the solid and fluid phases may be regarded as having the same temperature over length scales which are small compared with macroscopic scales, but which are large compared with the lengths associated with the microstructure of the porous medium. Many authors are now examining the ramifications of relaxing this assumption by allowing the temperatures of the phases to have different local temperatures. This does not mean that the fluid and the solid have different temperatures at their interfaces, but rather that the mean temperatures over a suitable representative elementary volume are not necessarily the same. Situations in which the two phases have markedly different thermal fields include cases of rapid changes in heating where the speed of the advancing thermal front is different in each phase, at least for short times; see [1]. They also include thermal boundary layer flows where cold fluid is entrained into the boundary layer which cools the fluid phase relative to the solid phase; see [2]. Detailed reviews of other research have been given recently by Kuznetsov [3] and Vafai and Amiri [4].

Pop and Yan [5] studied high Péclet number forced convective heat transfer past a cylinder which is held at uniform temperature and embedded in a porous medium. A thermal boundary layer is formed when the Péclet number is large and when local thermal equilibrium is valid. They found that it was possible to reduce the boundary layer equations to self-similar form and to obtain an analytical solution of the resulting equations. Rees et al. [6] solved the same problem but relaxed the assumption of local thermal equilibrium. In these cases the temperature field is no longer self-similar and it proves necessary to undertake the analysis numerically. It was found that thermal equilibrium is always attained at the rear stagnation point of the cylinder, but there could be very marked differences between the temperature fields of the fluid and solid phases at and near to the upstream stagnation point.

In this paper we also study forced convection flow past a heated horizontal circular cylinder but supplement the work of [6] by allowing the Péclet number to be finite. In this situation the governing equations for the temperature fields are no longer parabolic but are elliptic. Our problem is formulated in Section 2, the numerical scheme is presented briefly in Section 3, while the numerical results are displayed

* Corresponding author.
E-mail address: ensdasr@bath.ac.uk (D.A.S. Rees).
[1] Current address: Department of Mechanical Engineering, University of Sheffield, Sheffield, S10 2TN, UK.

1290-0729/$ – see front matter
doi:10.1016/j.ijthermalsci.2003.07.005

Nomenclature

a	radius of cylinder	m
c	specific heat	$kJ{\cdot}kg^{-1}{\cdot}K^{-1}$
h	solid/fluid heat transfer coefficient	$W{\cdot}m^{-3}{\cdot}K^{-1}$
H	nondimensional solid/fluid heat transfer coefficient	
k	thermal conductivity	$W{\cdot}m^{-1}{\cdot}K^{-1}$
K	permeability of the porous medium	m^2
LTE	local thermal equilibrium	
LTNE	local thermal nonequilibrium	
Nu	local Nusselt number	
$\bar{p}$	pressure	$kg{\cdot}m^{-1}{\cdot}s^{-2}$
Pe	Péclet number	
q	local rate of heat transfer	
Q	global rate of heat transfer	
r	radial coordinate	m
T	dimensional temperature	K
u	Darcy velocity in the r-direction	$m{\cdot}s^{-1}$
U	dimensional free stream velocity	$m{\cdot}s^{-1}$
v	Darcy velocity in the α-direction	$m{\cdot}s^{-1}$

Greek symbols

α	angular coordinate	
γ	modified conductivity ratio	
ε	porosity	
μ	fluid viscosity	$kg{\cdot}m^{-1}{\cdot}s^{-1}$
ρ	fluid density	$kg{\cdot}m^{-1}$
θ	temperature of fluid phase	
ϕ	temperature of solid phase	
ψ	streamfunction	

Subscripts

c	cylinder
f	fluid phase
s	solid phase
∞	ambient condition

Superscript

-	dimensional variable

and discussed in Section 4. A brief conclusion closes the paper.

2. Formulation of the problem

We consider the forced convection flow past a heated horizontal circular cylinder of radius, a, which is embedded in a porous medium. The dimensional free stream velocity is U and the temperatures of the cylinder and of the ambient fluid are T_c and T_∞, respectively, where $T_c > T_\infty$. The governing steady two-dimensional equations for forced convection flow are the equation of continuity,

$$\frac{\partial(\bar{r}\,\bar{u})}{\partial\bar{r}} + \frac{\partial\bar{v}}{\partial\alpha} = 0 \tag{1a}$$

the radial and angular momentum equations (Darcy's law),

$$\bar{u} = -\frac{K}{\mu}\frac{\partial\bar{p}}{\partial\bar{r}} \tag{1b}$$

$$\bar{v} = -\frac{K}{\mu}\frac{1}{\bar{r}}\frac{\partial\bar{p}}{\partial\alpha} \tag{1c}$$

and the respective energy equations for the fluid and solid phases,

$$\varepsilon k_f\left(\frac{\partial^2 T_f}{\partial\bar{r}^2} + \frac{1}{\bar{r}}\frac{\partial T_f}{\partial\bar{r}} + \frac{1}{\bar{r}^2}\frac{\partial^2 T_f}{\partial\alpha^2}\right) = (\rho c)_f\left(\bar{u}\frac{\partial T_f}{\partial\bar{r}} + \frac{\bar{v}}{\bar{r}}\frac{\partial T_f}{\partial\alpha}\right) + h(T_f - T_s) \tag{1d}$$

$$(1-\varepsilon)k_s\left(\frac{\partial^2 T_s}{\partial\bar{r}^2} + \frac{1}{\bar{r}}\frac{\partial T_s}{\partial\bar{r}} + \frac{1}{\bar{r}^2}\frac{\partial^2 T_s}{\partial\alpha^2}\right) = h(T_s - T_f) \tag{1e}$$

see [7]. In Eqs. (1) $\bar{u}$ and $\bar{v}$ denote the fluid flux velocities in the radial and tangential directions, $\bar{r}$ and α, respectively. The pressure is $\bar{p}$ and the temperature T and the subscripts f and s denote the fluid and solid phases, respectively.

Eq. (1) is nondimensionalised using the transformations

$$\bar{r} = ar \tag{2a}$$

$$(\bar{u}, \bar{v}) = U(u, v) \tag{2b}$$

$$T_f = (T_c - T_\infty)\theta + T_\infty \tag{2c}$$

$$T_s = (T_c - T_\infty)\phi + T_\infty \tag{2d}$$

We also introduce the stream-function, ψ, according to

$$u = \frac{1}{r}\frac{\partial\psi}{\partial\alpha} \tag{2e}$$

and

$$v = -\frac{\partial\psi}{\partial r} \tag{2f}$$

Eqs. (1) now reduce to

$$\frac{\partial^2\psi}{\partial r^2} + \frac{1}{r}\frac{\partial\psi}{\partial r} + \frac{1}{r^2}\frac{\partial^2\psi}{\partial\alpha^2} = 0 \tag{3a}$$

$$\frac{1}{Pe}\left[\frac{\partial^2\theta}{\partial r^2} + \frac{1}{r}\frac{\partial\theta}{\partial r} + \frac{1}{r^2}\frac{\partial^2\theta}{\partial\alpha^2}\right] = \frac{1}{r}\left[\frac{\partial\psi}{\partial\alpha}\frac{\partial\theta}{\partial r} - \frac{\partial\psi}{\partial r}\frac{\partial\theta}{\partial\alpha}\right] + H(\theta - \phi) \tag{3b}$$

$$\frac{1}{Pe}\left[\frac{\partial^2\phi}{\partial r^2} + \frac{1}{r}\frac{\partial\phi}{\partial r} + \frac{1}{r^2}\frac{\partial^2\phi}{\partial\alpha^2}\right] = H\gamma(\phi - \theta) \tag{3c}$$

where

$$H = \frac{ah}{U(\rho c)_f} \tag{4a}$$

$$\gamma = \frac{\varepsilon k_f}{(1-\varepsilon)k_s} \tag{4b}$$

and

$$Pe = \frac{Ua(\rho c)_f}{\varepsilon k_f} \tag{4c}$$

are dimensionless constants. Eq. (3) is subject to the boundary conditions

$$\psi = 0, \quad \theta = \phi = 1 \text{ on } r = 1 \quad \text{and}$$
$$\psi \to r\sin\alpha, \quad \theta, \phi \to 0 \text{ as } r \to \infty \tag{5}$$

In the above equations Pe is a Péclet number based on the fluid properties and scaled with the porosity, H represents the dimensionless interphase heat transfer coefficient and γ is a porosity-scaled conductivity ratio. Low values of γ generally correspond to a relatively poorly conducting fluid such as air in a metallic porous medium. For O(1) values of γ local thermal equilibrium corresponds to large values of H.

In nondimensional terms a uniform free stream is represented by $\psi = r\sin\alpha$. The appropriate solution of Eq. (3a) which yields the uniform stream when r is large is

$$\psi = \left(r - \frac{1}{r}\right)\sin\alpha \tag{6}$$

Thus Eqs. (3b) and (3c) become

$$\frac{1}{Pe}\left[\frac{\partial^2\theta}{\partial r^2} + \frac{1}{r}\frac{\partial\theta}{\partial r} + \frac{1}{r^2}\frac{\partial^2\theta}{\partial\alpha^2}\right] = \left(1 - \frac{1}{r^2}\right)\cos\alpha\,\frac{\partial\theta}{\partial r} - \left(\frac{1}{r} + \frac{1}{r^3}\right)\sin\alpha\,\frac{\partial\theta}{\partial\alpha} + H(\theta - \phi) \tag{7a}$$

$$\frac{1}{Pe}\left[\frac{\partial^2\phi}{\partial r^2} + \frac{1}{r}\frac{\partial\phi}{\partial r} + \frac{1}{r^2}\frac{\partial^2\phi}{\partial\alpha^2}\right] = H\gamma(\phi - \theta) \tag{7b}$$

Numerical solutions are presented in subsequent sections in the form of both local and global rates of heat transfer. The local rates of heat transfer are given by

$$q_f = -\left.\frac{\partial\theta}{\partial r}\right|_{r=1}, \qquad q_s = -\left.\frac{\partial\phi}{\partial r}\right|_{r=1} \tag{8}$$

while the global rates of heat transfer, which are defined as the local values averaged between $\alpha = 0$ and $\alpha = \pi$, are then given by

$$Q_f = -\frac{1}{\pi}\int_0^\pi \left.\frac{\partial\theta}{\partial r}\right|_{r=1} \mathrm{d}\alpha \tag{9a}$$

and

$$Q_s = -\frac{1}{\pi}\int_0^\pi \left.\frac{\partial\phi}{\partial r}\right|_{r=1} \mathrm{d}\alpha \tag{9b}$$

3. Numerical method

Eq. (7) was solved by means of second-order accurate central difference approximations. As iterative methods often need substantial under-relaxation to guarantee convergence when parameters like the Péclet number are large, it was decided to employ a time-stepping method and therefore straightforward first-order time derivatives were added to the right-hand sides of Eq. (7) to form an unsteady system of equations. Time stepping was undertaken using the DuFort–Frankel method, details of which may be found in many textbooks, such as that of Smith [8].

Only half the physical domain was used because the line $\alpha = 0, \pi$ is a line of symmetry, and, therefore, the first α-derivative of both θ and ϕ were set to zero at $\alpha = 0$ and π. The external boundary, located at a suitably large value of r, is both an inflow and an outflow boundary. Fluid flows in the range $\frac{1}{2}\pi < \alpha < \pi$ and, therefore, we set $\theta = \phi = 0$ on that part of the boundary. In the range $0 \leqslant \alpha < \frac{1}{2}\pi$ fluid flows out and, therefore, the choice of boundary condition is more difficult since neither the temperatures nor their first r-derivatives are likely to be zero. Two different methods were used:

(i) the second derivative with respect to r was set to zero, and
(ii) a buffer region methodology was adopted.

The first method was not found to be uniformly good and occasionally there were difficulties with pointwise spatial oscillations near outflow, and with lack of convergence to the steady state. The second method is drawn from recent work on the direct numerical simulation of boundary layer instabilities where disturbances to the basic flow are artificially damped out by multiplying the disturbance field by an appropriate function (which is equal to 1 over most of the computational domain, but which decreases smoothly to 0 at the outflow boundary); see [9]. While this method was designed for those boundary layer instabilities which are absolute instabilities, we found that it also works well in the present context when the outer boundary is sufficiently far from the cylinder. Surface rates of heat transfer were found to vary only very slightly indeed between different sizes of domain, and while the buffer region does modify the temperature field locally, it has negligible upstream effect. In fact, there is little difference in the results obtained between methods (i) and (ii) except for near the outflow boundary. However, it was found that method (ii) was more robust.

The distance the thermal field penetrates into the surrounding porous medium depends very strongly on the values of Pe and H, in particular, and, therefore, the maximum value of r used in the numerical simulations varied very considerably. For large values of Pe and H the value $r_{\max} = 3$ was sufficient, whereas when Pe and H are relatively small $r_{\max}$ was sometimes greater than 100. In almost all cases the number grid points in the α-direction was 160. The size of the time-step is immaterial since the aim is to determine the resulting steady-state flow-field as efficiently as possible.

4. Numerical solutions

There are three governing parameters which may vary independently, *Pe*, H and γ. In Figs. 1–4 we display the detailed isotherms for various cases, which illustrate the full behaviour of the forced convection temperature fields. In these figures the isotherms corresponding to the fluid phase are displayed in the upper half, while the lower half is reserved for the solid phase isotherms.

Fig. 1 shows how the thickness of the thermal region varies with Péclet when $H = \gamma = 1$. When *Pe* is small, then conduction is much more significant than advection, at least near the cylinder, and, therefore, there is an appreciable conduction against the flow upstream of the cylinder. As *Pe* increases, advection becomes increasingly dominant. A thermal boundary forms on the upstream side of the cylinder accompanied by increasing rates of heat transfer. When the Péclet number reaches 1000 the boundary layer has progressed much further round the cylinder, following the flow, and is clearly evident on the downstream side. At such values of H and γ, local thermal nonequilibrium (LTNE) effects are quite noticeable but are not too large, and may be seen most easily on the upstream side for $Pe = 10$ and $Pe = 100$. They remain significant at $Pe = 1000$ and higher, but it is difficult to see them with the eye; that they remain significant has already been shown in [2]. On the other hand, when *Pe* becomes small, then local thermal equilibrium (LTE) is recovered gradually, as may be seen by the small mismatch between the isotherms on the $\alpha = \pi$ axis. At such small values conduction dominates, and the terms multiplying H in Eq. (7) are of O(*Pe*) relative to the conduction terms.

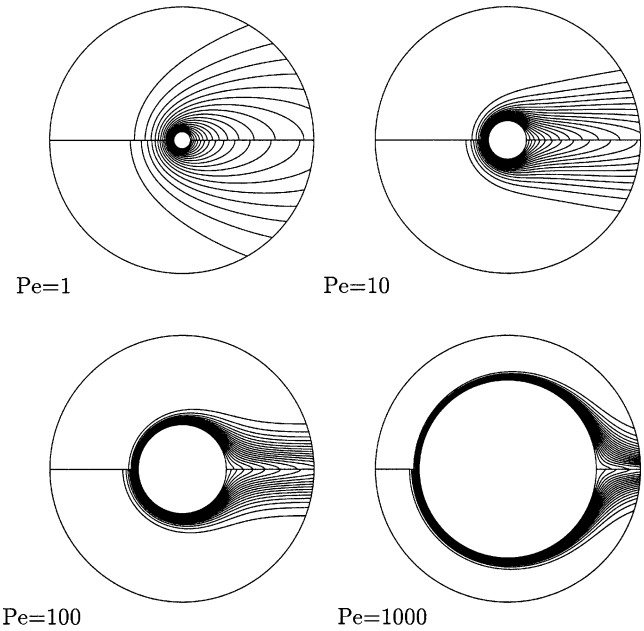

Fig. 1. Isotherm plots for forced convection past a uniform temperature cylinder with $H = \gamma = 1$. Isotherms for the fluid phase occupy the upper half of each subfigure while the lower half corresponds to the solid phase. Isotherms are plotted at intervals of 0.05; this convention also applies to Figs. 2–4. The values of the Péclet number are, 1, 10, 100, 1000.

Fig. 2 corresponds to variations in H when $Pe = 100$ and $\gamma = 1$, and the aim here is to see the effect of changes in the ease with which heat may be transferred between the phases. When $H = 0.01$ there is a considerable difference in the spatial extent of the thermal fields since conductive effects dominate the movement of heat in the solid phase, since Eq. (7) for θ and ϕ is almost decoupled. Increasing the value of H serves to allow a greater transfer of heat from the solid phase into the fluid phase. As a result of this the thickness of the fluid phase boundary layer increases slightly as H increases while that of the solid phase decreases until they become identical at large values of H. We see that there remains a slight mismatch between the isotherms of the respective phases on the $\alpha = 0$ axis when $H = 10$, but this has disappeared when $H = 100$.

Similar variations in H are shown in Fig. 3 where we have reduced the value of the Péclet number to $Pe = 1$. The strength of the external flow is now 0.01 of the strength of that corresponding to Fig. 2 and, therefore, the isotherms extend much further from the cylinder in both phases for otherwise identical parameters. Once more, we see the facts that the solid phase isotherms extend considerably further than those of the fluid phase when H is small, and that the thermal become identical when H becomes large.

The final set of isotherms shown here are given in Fig. 4 where we see the effect of changes in γ for $Pe = 100$ and $H = 1$. For all values of γ which are shown there is a slight difference between the thermal fields of the phases, although this disappears when γ is large. In such cases the solid field may be seen, from Eq. (7b), to differ from the fluid field by an amount which is $O(\gamma^{-1})$, and, therefore, we have LTE in the limit of large γ even though $H = 1$. However, when γ is small, the temperature of the solid phase is affected much more by conduction as the term coupling the phases in (7b) is of $O(\gamma)$. On the other hand, the corresponding term in (7a) remains of O(1) and, therefore, the extent of the thermal field of the fluid phase expands to follow that of the solid phase.

Figs. 5–8 show local rates of heat transfer which correspond to the isotherm plots displayed in Figs. 1–4, respectively. All these figures show very clearly how small the local rate of heat transfer is at the rear stagnation point, where the developing thermal lifts off the cylinder, compared with the upstream stagnation point. This is especially true when *Pe* is large, as shown in Figs. 5 and 6, in general.

In all cases the local heat transfer of the fluid phase is higher than that of the solid phase over most of the cylinder and including the upstream stagnation point. Close to the downstream stagnation point the fluid phase has the smaller rate of heat transfer since conduction is assisted by advection. This is seen most clearly in Figs. 6 and 7 for which $Pe = 100$ and $Pe = 1$, respectively, and different curves correspond to different values of H.

In both Figs. 6 and 7 the difference between cases for which H is small and those for which H is large is quite

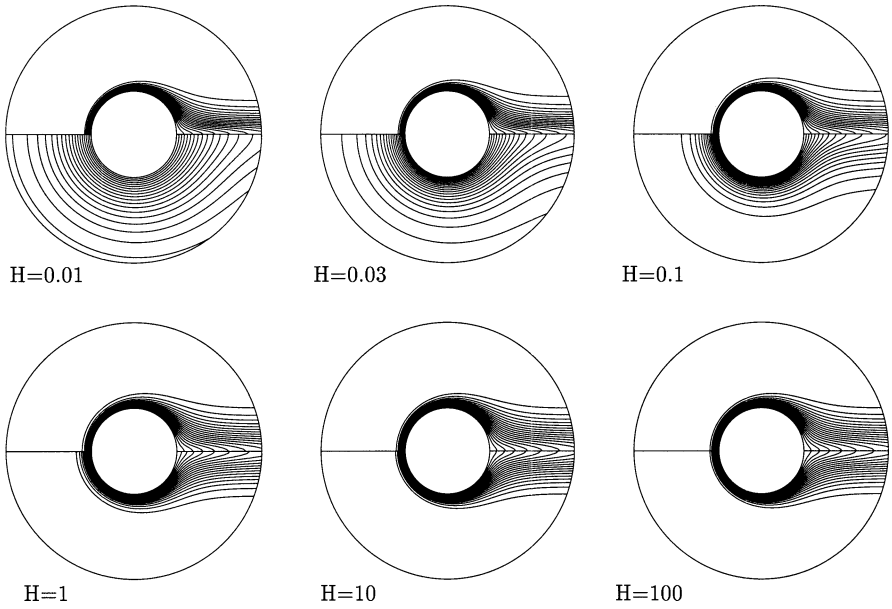

Fig. 2. The effect of different values of H on the isotherms for $Pe = 100$ and $\gamma = 1$. The parameter H takes the values 0.01, 0.03, 0.1, 1, 10 and 100.

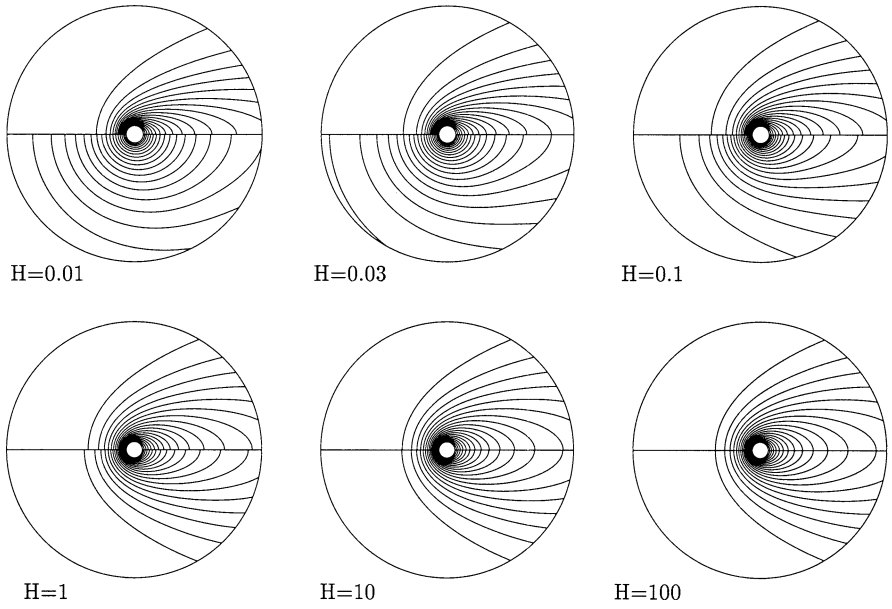

Fig. 3. The effect of different values of H on the isotherms for $Pe = 1$ and $\gamma = 1$. The parameter H takes the values 0.01, 0.03, 0.1, 1, 10 and 100.

dramatic. At large values of H the variations of q_f and q_s are very similar and differ by little. But, when H is small, q_s varies only slightly, confirming the dominance of conduction, at least close to the cylinder itself. On the other hand, q_f still varies in the same manner as when H is large, but with a slightly increased magnitude.

Similar comments apply when we consider variations in γ, as shown in Fig. 8. Small values of γ cause q_s to vary only slightly with position around the cylinder, while the opposite is true when γ is large.

Finally, we consider some detailed values of the global rates of heat transfer. The numbers displayed in each table have errors which are less than 1%; higher accuracy can be obtained by either using a much finer grid, which will take considerably more CPU time, or by using more sophisticated methods.

Table 1 shows how Q_f and Q_s vary with H when $H = \gamma = 1$. The increase in the rate of heat transfer with *Pe* is very evident, but it is worth noting that there is an approximately tenfold increase in both Q_f and Q_s as *Pe* increases from 10 to 1000. This is consistent with the boundary layer analysis of [6] where the local and global rates of heat transfer were found to be proportional to $Pe^{1/2}$ when *Pe* is large. The last two columns of Table 1 show how $Q_f/Pe^{1/2}$ and $Q_s/Pe^{1/2}$ vary, and serves as check on the accuracy of the present computations. In [6] it was found that $Q_f/Pe^{1/2} = 0.5858$

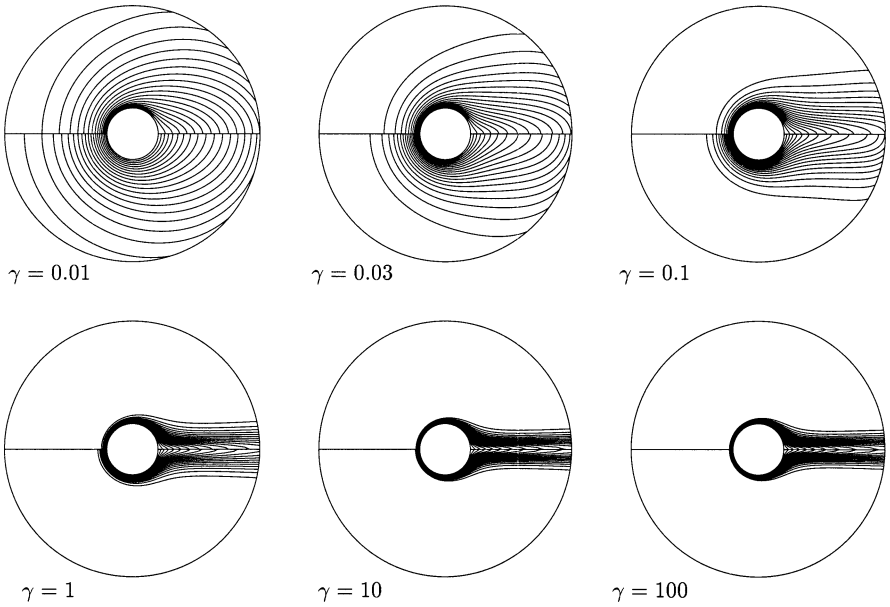

Fig. 4. The effect of different values of γ on the isotherms for $Pe = 100$ and $H = 1$. The parameter γ takes the values 0.01, 0.03, 0.1, 1, 10 and 100.

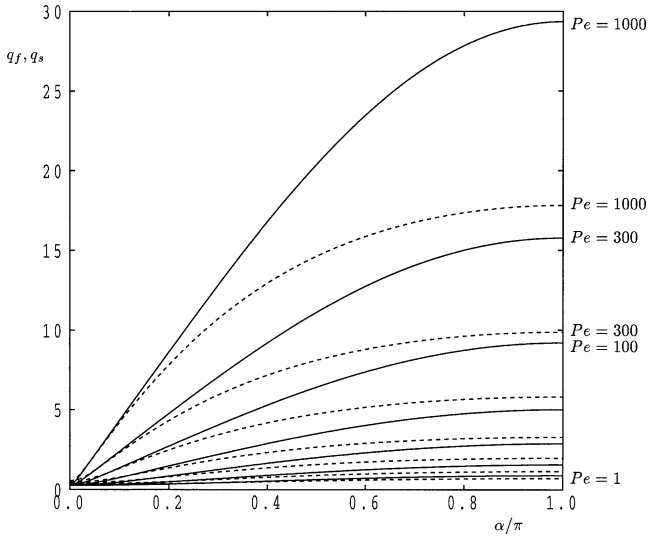

Fig. 5. Values of q_f (continuous lines) and q_s (dashed lines) as functions of α for $H = \gamma = 1$ and $Pe = 1, 3, 10, 30, 100, 300$ and 1000. At $\alpha = \pi$ both q_f and q_s increase with Pe.

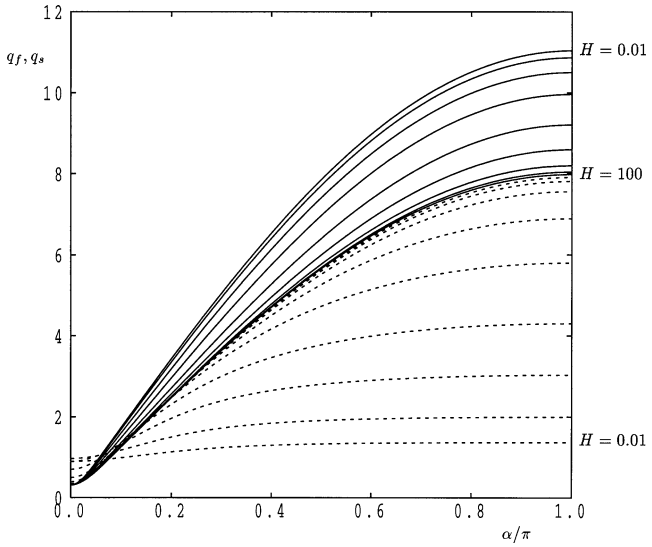

Fig. 6. Values of q_f (continuous lines) and q_s (dashed lines) as functions of α for $Pe = 100$ and $\gamma = 1$ with $H = 0.01, 0.03, 0.1, 0.3, 1, 3, 10, 30$ and 100. At $\alpha = \pi$ both q_f and q_s vary monotonically with H.

and $Q_s/Pe^{1/2} = 0.3976$ in the large Péclet number limit. Therefore, we conclude that our present computations are consistent with boundary layer theory.

Tables 2 and 3 show the variations of Q_f and Q_s with H when $\gamma = 1$ and when $Pe = 100$ and $Pe = 1$, respectively. The tendency noted earlier for LTE to be established as H increases may be seen clearly since the ratio $Q_f/Q_s \to 1$ in this limit. It is also worthy of note that the degree of LTNE not only decreases when H increases for fixed values of Pe, but also as Pe decreases for fixed values of H. This latter may be understood because the increasing dominance of conduction as the primary mechanism of heat transfer near the surface allows the phases more room in which to become more equal. Mathematically, this is equivalent to the decreasing the effect of advection near the surface since

Table 1
Values of Q_f and Q_s as a function of Pe when $H = \gamma = 1$

Pe	Q_f	Q_s	$Q_f/Pe^{1/2}$	$Q_s/Pe^{1/2}$
1	0.6097	0.5391		
3	1.0145	0.8337		
10	1.8290	1.4049	0.5784	0.4443
30	3.1727	2.3358	0.5793	0.4265
100	5.8203	4.1463	0.5820	0.4146
300	10.1007	7.1209	0.5832	0.4111
1000	18.5219	12.7876	0.5857	0.4044

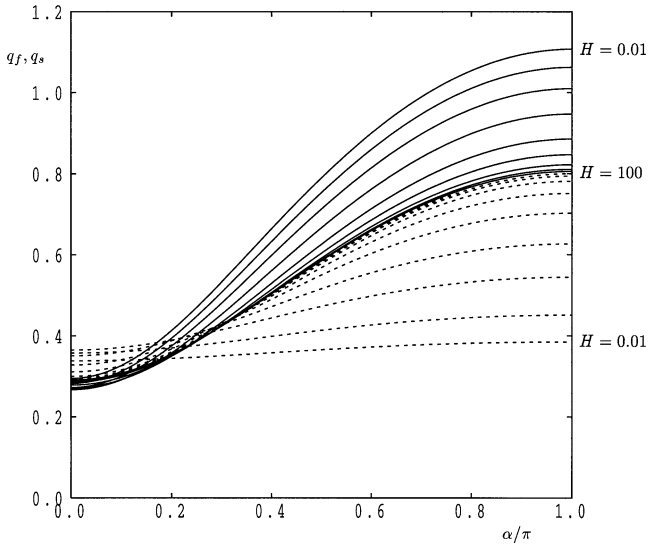

Fig. 7. Values of q_f (continuous lines) and q_s (dashed lines) as functions of α for $Pe = 1$ and $\gamma = 1$ with $H = 0.01, 0.03, 0.1, 0.3, 1, 3, 10, 30$ and 100. At $\alpha = \pi$ both q_f and q_s vary monotonically with H.

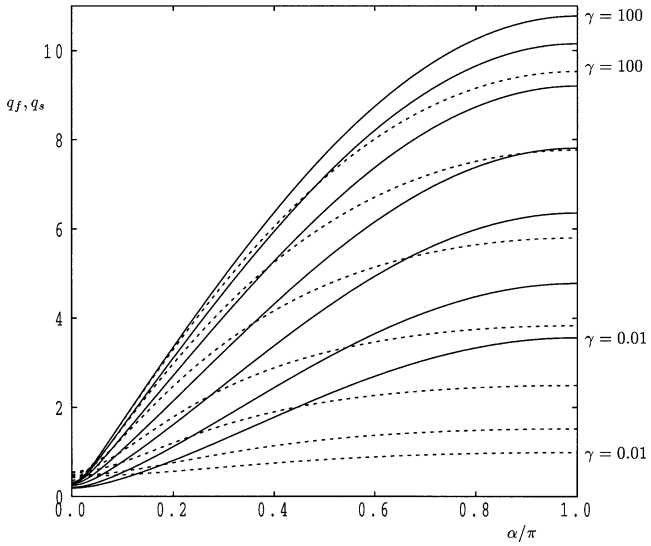

Fig. 8. Values of q_f (continuous lines) and q_s (dashed lines) as functions of α for $Pe = 100$ and $H = 1$ with $\gamma = 0.01, 0.03, 0.1, 0.3, 1, 3, 10, 30$ and 100. At $\alpha = \pi$ both q_f and q_s increase with γ.

these terms are of O(*Pe*) relative to the conduction terms, thereby rendering Eqs. (7a) and (7b) identical at leading order in *Pe*.

Table 4 shows the effect of varying γ when $Pe = 100$ and $H = 1$. The primary effect, as noted earlier, of small values of γ is to caused the thermal fields of both phases to expand relative to when γ is large, and, therefore, the associated global rates of heat transfer decrease as γ decreases. It may also be seen that LTNE also becomes stronger in that limit, which suggests that thermal conduction in the solid phases becomes significant.

Table 2
Values of Q_f and Q_s as a function of H when $Pe = 100$ and $\gamma = 1$

H	Q_f	Q_s	Q_f/Q_s
0.01	7.0934	1.2614	5.6236
0.03	6.9671	1.7620	3.9540
0.1	6.7028	2.5122	2.6681
0.3	6.3191	3.3199	1.9034
1	5.8203	4.1463	1.4038
3	5.4520	4.6652	1.1687
10	5.2326	4.9492	1.0573
30	5.1514	5.0503	1.0200
100	5.1200	5.0888	1.0061

Table 3
Values of Q_f and Q_s as a function of H when $Pe = 1$ and $\gamma = 1$

H	Q_f	Q_s	Q_f/Q_s
0.01	0.7554	0.3683	2.0510
0.03	0.7224	0.4141	1.7445
0.1	0.6858	0.4695	1.4607
0.3	0.6449	0.5086	1.2679
1	0.6096	0.5391	1.1308
3	0.5906	0.5564	1.0614
10	0.5799	0.5661	1.0244
30	0.5756	0.5700	1.0097
100	0.5737	0.5718	1.0033

Table 4
Values of Q_f and Q_s as a function of γ when $Pe = 100$ and $H = 1$

γ	Q_f	Q_s	Q_f/Q_s
0.01	2.1141	0.7835	2.6983
0.03	2.8577	1.1574	2.4691
0.1	3.8737	1.8775	2.0632
0.3	4.8472	2.8338	1.7105
1	5.8203	4.1463	1.4038
3	6.4880	5.3536	1.2119
10	6.9179	6.3510	1.0893
30	7.0970	6.8541	1.0354
100	7.1717	7.0894	1.0116

5. Conclusions

In this paper we have examined the steady forced convection boundary layer flow past a hot cylinder which is embedded in a fluid-saturated porous medium where a two-temperature model of the microscopic heat transfer between the solid and fluid phases has been adopted. Detailed results for a representative sets of parameters has been presented in a variety of forms: isotherm plots, variation of local rates of heat transfer, and values of global rates of heat transfer.

When the Péclet number is large we find that our results compare very favourably with the boundary layer analysis of [6]. At small values of *Pe* the thermal field of both phases spreads a considerable distance from the cylinder, and it is hoped to be able to perform a small-*Pe* analysis of this situation in the future.

In general, the local rate of heat transfer decreases with distance around the cylinder from the upstream stagnation

point. Initially, the value of q_s is less than that of q_f because the thermal field of the solid phase is not affected directly by the oncoming stream and conducts a greater distance upstream. However, further around the cylinder, where the main flow is tangential to the cylinder, heat begins to be advected strongly away from the cylinder in the fluid phase and therefore $q_f < q_s$ in the region near the downstream stagnation point.

It was found that LTE is established in the following separate limits: $H \to \infty$, $\gamma \to \infty$ and $Pe \to 0$. The first two of these have also been found in many other studies, but the third is rather unusual. As noted above, the small-*Pe* limit corresponds to the dominance of conduction as a mechanism of heat transfer near the cylinder since Eqs. (7a) and (7b) are identical at leading order in each phase when $Pe \ll 1$.

References

[1] W.J. Minkowycz, A. Haji-Sheikh, K. Vafai, On departure from local thermal equilibrium in porous media due to a rapidly changing heat source: the Sparrow number, Internat. J. Heat Mass Transfer 42 (1999) 3373–3385.

[2] D.A.S. Rees, I. Pop, Vertical free convection boundary layer flow in a porous medium using a thermal nonequilibrium model, J. Porous Media 3 (2000) 31–44.

[3] A.V. Kuznetsov, Thermal nonequilibrium forced convection in porous media, in: D.B. Ingham, I. Pop (Eds.), Transport Phenomena in Porous Media, Pergamon, Oxford, 1998, pp. 103–129.

[4] K. Vafai, A. Amiri, Non-Darcian effects in combined forced convective flows, in: D.B. Ingham, I. Pop (Eds.), Transport Phenomena in Porous Media, Pergamon, Oxford, 1998, pp. 313–329.

[5] I. Pop, B. Yan, Forced convection flow past a cylinder and a sphere in a Darcian fluid at large Péclet numbers, Internat. Comm. Heat Mass Transfer 25 (1998) 261–267.

[6] D.A.S. Rees, A.P. Bassom, I. Pop, Forced convection past a heated cylinder in a porous medium using a thermal nonequilibrium model: boundary layer analysis. Eur. J. Mech. B. Fluids, submitted for publication.

[7] D.A. Nield, A. Bejan, Convection in Porous Media, second ed., Springer, New York, 1999.

[8] G.D. Smith, Numerical Solution of Partial Differential Equations: Finite Difference Methods, second ed., OUP, Oxford, 1978.

[9] M. Kloker, U. Konzelmann, H. Fasel, Outflow boundary conditions for spatial Navier–Stokes simulations of transitional boundary-layers, AIAA J. 31 (1993) 620–628.